

Orbital Angular Momentum of Magnons in Collinear Magnets

Randy S. Fishman[✉],* Jason S. Gardner, and Satoshi Okamoto[✉]

Materials Science and Technology Division, Oak Ridge National Laboratory, Oak Ridge, Tennessee 37831, USA

 (Received 28 March 2022; revised 28 July 2022; accepted 19 September 2022; published 13 October 2022)

We study the orbital angular momentum of magnons for collinear ferromagnet (FM) and antiferromagnetic (AF) systems with nontrivial networks of exchange interactions. The orbital angular momentum of magnons for AF and FM zigzag and honeycomb lattices becomes nonzero when the lattice contains two inequivalent sites and is largest at the avoided-crossing points or extremum of the frequency bands. Hence, the arrangement of exchange interactions may play a more important role at producing the orbital angular momentum of magnons than the spin-orbit coupling energy and the resulting noncollinear arrangement of spins.

DOI: [10.1103/PhysRevLett.129.167202](https://doi.org/10.1103/PhysRevLett.129.167202)

For more than a century, scientists have been intrigued by the conversion of spin into orbital angular momentum (OAM) and vice versa. In 1915, Einstein and de Haas [1] demonstrated that a change of magnetization can cause the container of that magnet to rotate. Also in 1915, Barnett [2] demonstrated that the rotation of electrons can be converted into magnetization. In solids, the conversion of spin into orbital angular momentum is produced by the spin-orbit (SO) coupling. Recently, scientists have been searching for evidence of OAM [3,4] in spin excitations, also known as magnons. Whereas a magnon corresponding to a single spin flip has spin $S = \pm\hbar$, the OAM \mathcal{L} of such a magnon is unknown.

Two main approaches have been employed to search for the OAM of magnons. Because SO coupling is also responsible for Dzyaloshinskii-Moriya (DM) interactions, Neumann *et al.* [5] examined the OAM of magnons associated with the noncollinear spin states produced by DM interactions. Other groups have investigated the OAM of magnons in confined geometries. In a whispering gallery mode cavity, for example, circulating magnons with perpendicular OAM can be excited on the surface of a FM sphere by incident light [6–8]. Magnons with a range of orbital quantum numbers have been predicted for a FM nanocylinder that hosts a skyrmion at one end [9] and for a skyrmion-textured domain wall in a FM nanotube [10]. Quantum confinement of magnons has also been observed in a ferrite disk placed inside a microwave cavity [11]. While approaches based on both SO coupling and confined geometries have achieved some success, they also require complex experiments and theories. In a seemingly unrelated approach, Matsumoto and Murakami [12] developed an expression for the OAM of FM magnons due to their “self-rotation,” which on average is opposed by the contribution of magnons to the edge current [13,14].

This Letter demonstrates that collinear magnets with tailored exchange geometries can generate magnons that

exhibit OAM. Results for both FM and AF zigzag and honeycomb lattices in two dimensions indicate that the OAM becomes nonzero when the lattice contains two inequivalent sites and is greatest at the avoided-crossing points or extremum of the magnon bands. For FM zigzag chains, the OAM vanishes when the upper and lower bands cross but becomes quite large when the gap between the bands is small but nonzero. For FM honeycomb lattices, the upper and lower bands carry opposite OAM when averaged over the Brillouin zone (BZ). For AF honeycomb lattices, the two degenerate magnon bands can be divided into major and minor branches that carry different OAM. We shall see that the OAM and Berry curvature [15] capture different but related aspects of the magnon band topology.

Formally, the classical equations of motion [16,17] for the dynamical magnetization $\boldsymbol{\mu}_i = 2\mu_B\delta\mathbf{S}_i$ at site i produce the linear momentum \mathbf{p}_i [18]:

$$p_{i\alpha} = \frac{1}{4\mu_B M_0} (\boldsymbol{\mu}_i \times \mathbf{n}_i) \cdot \frac{\partial \boldsymbol{\mu}_i}{\partial x_\alpha}, \quad (1)$$

where $M_0 = 2\mu_B S$ is the static magnetization for a spin \mathbf{S}_i pointing along \mathbf{n}_i (a derivation of the classical OAM is provided in the Supplemental Material [19]). Using the $1/S$ quantization conditions $\bar{\mu}_i^+ = \mu_{ix}n_{iz} + i\mu_{iy} = 2\mu_B\sqrt{2S\hbar}a_i$ and $\bar{\mu}_i^- = \mu_{ix}n_{iz} - i\mu_{iy} = 2\mu_B\sqrt{2S\hbar}a_i^\dagger$ for the dynamical magnetization in terms of the local Boson operators a_i and a_i^\dagger satisfying the momentum-space commutation relations $[a_{\mathbf{k}}^{(r)}, a_{\mathbf{k}'}^{(s)\dagger}] = \delta_{rs}\delta_{\mathbf{k},\mathbf{k}'}$ and $[a_{\mathbf{k}}^{(r)}, a_{\mathbf{k}'}^{(s)}] = 0$, the quantized OAM along \mathbf{z} is given by

$$\begin{aligned} \mathcal{L}_z &= \sum_i (\mathbf{r}_i \times \mathbf{p}_i) \cdot \mathbf{z} \\ &= \frac{\hbar}{2} \sum_{r=1}^M \sum_{\mathbf{k}} \{a_{\mathbf{k}}^{(r)} \hat{l}_{z\mathbf{k}} a_{\mathbf{k}}^{(r)\dagger} - a_{\mathbf{k}}^{(r)\dagger} \hat{l}_{z\mathbf{k}} a_{\mathbf{k}}^{(r)}\}, \quad (2) \end{aligned}$$

where r and s refer to the M sites in the magnetic unit cell and

$$\hat{l}_{z\mathbf{k}} = -i \left(k_x \frac{\partial}{\partial k_y} - k_y \frac{\partial}{\partial k_x} \right) \quad (3)$$

is the OAM operator. Transforming to the Boson operators $b_{\mathbf{k}}^{(n)}$ and $b_{\mathbf{k}}^{(n)\dagger}$ that diagonalize the Hamiltonian H , we define [20]

$$\begin{aligned} a_{\mathbf{k}}^{(r)} &= \sum_n \{ X^{-1}(\mathbf{k})_{rn} b_{\mathbf{k}}^{(n)} + X^{-1}(\mathbf{k})_{r,n+M} b_{-\mathbf{k}}^{(n)\dagger} \}, \\ a_{-\mathbf{k}}^{(r)\dagger} &= \sum_n \{ X^{-1}(\mathbf{k})_{r+M,n} b_{\mathbf{k}}^{(n)} + X^{-1}(\mathbf{k})_{r+M,n+M} b_{-\mathbf{k}}^{(n)\dagger} \}. \end{aligned} \quad (4)$$

The zero-temperature expectation value of \mathcal{L}_z for magnon state $b_{\mathbf{k}}^{(n)\dagger}|0\rangle = |\mathbf{k}, n\rangle$ with frequency $\omega_n(\mathbf{k})$ is

$$\begin{aligned} \mathcal{L}_{zn}(\mathbf{k}) &= \langle \mathbf{k}, n | \mathcal{L}_z | \mathbf{k}, n \rangle \\ &= \frac{\hbar}{2} \sum_{r=1}^M \{ X^{-1}(\mathbf{k})_{rn} \hat{l}_{z\mathbf{k}} X^{-1}(\mathbf{k})_{rn}^* \\ &\quad - X^{-1}(\mathbf{k})_{r+M,n} \hat{l}_{z\mathbf{k}} X^{-1}(\mathbf{k})_{r+M,n}^* \}. \end{aligned} \quad (5)$$

For collinear spin states *without* DM interactions, $\underline{X}^{-1}(-\mathbf{k}) = \underline{X}^{-1}(\mathbf{k})^*$ so that $\mathcal{L}_{zn}(\mathbf{k}) = -\mathcal{L}_{zn}(-\mathbf{k})$ is an odd function of \mathbf{k} .

(i) *FM zigzag*.—Our first case study is the square lattice shown in Fig. 1(a) with alternating FM bonds $J_1 > 0$ and $J_2 > 0$ coupling sites 1 and 2 with spins up. Second order in the operator $\mathbf{v}_{\mathbf{k}} = (a_{\mathbf{k}}^{(1)}, a_{\mathbf{k}}^{(2)}, a_{-\mathbf{k}}^{(1)\dagger}, a_{-\mathbf{k}}^{(2)\dagger})$, the Hamiltonian $H_2 = \sum_{\mathbf{k}} \mathbf{v}_{\mathbf{k}}^\dagger \cdot \underline{L}(\mathbf{k}) \cdot \mathbf{v}_{\mathbf{k}}$ is defined in terms of the matrix

$$\underline{L}(\mathbf{k}) = (J_1 + J_2) S \begin{pmatrix} 1 & -\Psi_{\mathbf{k}}^* & 0 & 0 \\ -\Psi_{\mathbf{k}} & 1 & 0 & 0 \\ 0 & 0 & 1 & -\Psi_{\mathbf{k}}^* \\ 0 & 0 & -\Psi_{\mathbf{k}} & 1 \end{pmatrix}, \quad (6)$$

where $\Psi_{\mathbf{k}} = (J_1 \xi_{\mathbf{k}}^* + J_2 \xi_{\mathbf{k}}) / 2(J_1 + J_2)$ with $\xi_{\mathbf{k}} = \exp(ik_x a) + \exp(ik_y a)$. To study the magnon dynamics, we must diagonalize $\underline{L} \cdot \underline{N}$, where

$$\underline{N} = \begin{pmatrix} \underline{I} & 0 \\ 0 & -\underline{I} \end{pmatrix} \quad (7)$$

and \underline{I} is the two-dimensional identity matrix. Using the relation $\underline{N} \cdot \underline{X}^\dagger(\mathbf{k}) \cdot \underline{N} = \underline{X}^{-1}(\mathbf{k})$ to normalize the eigenvectors [20] $X^{-1}(\mathbf{k})_{rn}$, we find

$$\underline{X}^{-1}(\mathbf{k}) = \frac{1}{\sqrt{2}|\Psi_{\mathbf{k}}^*|} \begin{pmatrix} -\Psi_{\mathbf{k}}^* & \Psi_{\mathbf{k}}^* & 0 & 0 \\ |\Psi_{\mathbf{k}}| & |\Psi_{\mathbf{k}}| & 0 & 0 \\ 0 & 0 & -\Psi_{\mathbf{k}}^* & \Psi_{\mathbf{k}}^* \\ 0 & 0 & |\Psi_{\mathbf{k}}| & |\Psi_{\mathbf{k}}| \end{pmatrix}. \quad (8)$$

It is then simple to show that

$$\mathcal{L}_{zn}(\mathbf{k}) = \frac{\hbar}{4} \frac{\Psi_{\mathbf{k}}}{|\Psi_{\mathbf{k}}|} \hat{l}_{z\mathbf{k}} \frac{\Psi_{\mathbf{k}}^*}{|\Psi_{\mathbf{k}}|} \quad (9)$$

is the same for magnon bands $n = 1$ and 2 with energies $\hbar\omega_{1,2}(\mathbf{k}) = (J_1 + J_2)S(1 \pm |\Psi_{\mathbf{k}}|)$.

Results for $\mathcal{L}_{zn}(\mathbf{k})/\hbar$ are plotted as a function of $r = J_2/J_1$ in Fig. 1(c) [21]. Not surprisingly, $\mathcal{L}_{zn}(\mathbf{k})$ vanishes for a square-lattice FM with $r = 1$. Comparing the ‘‘hot spots’’ in Fig. 1(c) for $r = 1.1$ with the magnon bands in Fig. 1(b) for $k_y a/2\pi = 0.1$, we see that the OAM is largest ($\sim 2\hbar$) at the avoided-crossing points \mathbf{k}^* of bands 1 and 2 near $k_x a/2\pi = 0.4$. As r increases, the gap between the bands grows, the region of large $|\mathcal{L}_{zn}(\mathbf{k})|$ spreads out in \mathbf{k} space, and its amplitude decreases. For very large r , the regions of large positive and negative $\mathcal{L}_{zn}(\mathbf{k})$ stretch into stripes. The wave vectors \mathbf{k}^* are associated with a sign change in the Berry curvature [15,19].

(ii) *AF zigzag*.—For the square lattice in Fig. 2(a), we take $J_1 < 0$ and $J_2 > 0$ so that sites 1 and 2 have spins up while sites 3 and 4 have spins down. Although $\underline{L}(\mathbf{k})$ is eight dimensional, it breaks into the two identical 4×4 matrices

$$\underline{L}(\mathbf{k})' = (J_2 - J_1) S \begin{pmatrix} 1 & -\gamma_2 \xi_{\mathbf{k}} & 0 & \gamma_1 \xi_{\mathbf{k}}^* \\ -\gamma_2 \xi_{\mathbf{k}}^* & 1 & \gamma_1 \xi_{\mathbf{k}} & 0 \\ 0 & \gamma_1 \xi_{\mathbf{k}}^* & 1 & -\gamma_2 \xi_{\mathbf{k}} \\ \gamma_1 \xi_{\mathbf{k}} & 0 & -\gamma_2 \xi_{\mathbf{k}}^* & 1 \end{pmatrix} \quad (10)$$

with doubly degenerate magnon energies

$$\begin{aligned} \hbar\omega_{1,2}(\mathbf{k}) &= 2(J_2 - J_1) S \{ 1 - (\gamma_1^2 - \gamma_2^2) |\xi_{\mathbf{k}}|^2 \\ &\quad \pm \gamma_2 \sqrt{\gamma_1^2 (\xi_{\mathbf{k}}^2 - \xi_{\mathbf{k}}^*)^2 + 4 |\xi_{\mathbf{k}}|^2} \}^{1/2}, \end{aligned} \quad (11)$$

where $\gamma_n = J_n / 2(J_2 - J_1)$.

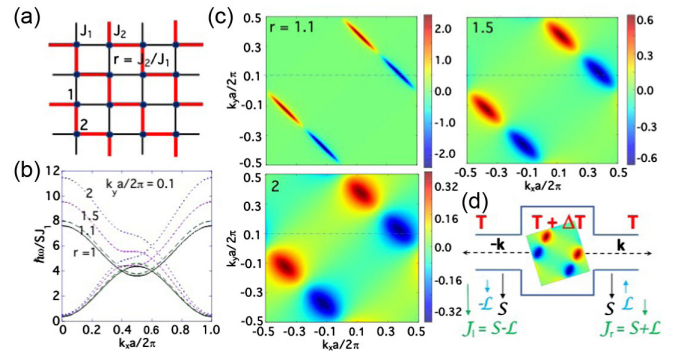


FIG. 1. FM zigzag. (a) A square lattice with alternating FM exchange interactions J_1 and J_2 between up spins. (b) Magnon bands for $k_y a/2\pi = 0.1$. (c) The OAM $\mathcal{L}_{zn}(\mathbf{k})/\hbar$ graphed as a function of \mathbf{k} for different values of $r = J_2/J_1$. The dashed line shows $k_y a/2\pi = 0.1$. (d) Magnons of an $r = 2$ FM zigzag material traveling with opposite momenta $\pm \mathbf{k}$ and OAM $\pm \mathcal{L}$ in a temperature gradient.

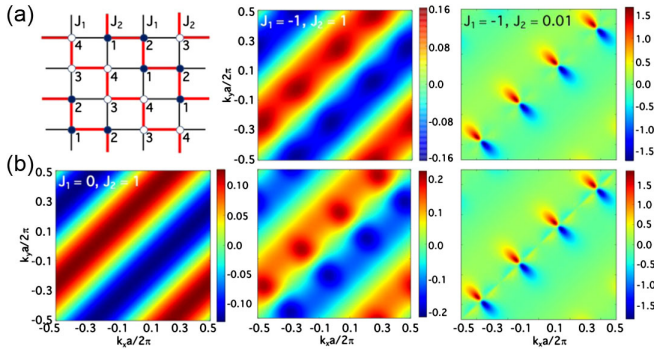


FIG. 2. AF zigzag. (a) A square lattice with FM exchange $J_2 > 0$ on zigzag chains with up (closed circles) or down (open circles) spins coupled by AF exchange $J_1 < 0$. (b) The OAM for upper (top) and lower (bottom) bands versus \mathbf{k} for different values of J_1 and J_2 .

While no simple analytic expression for the OAM is possible, we readily obtain the numerical solutions in Fig. 2(b). For $J_1 = 0$, the zigzag chains are isolated from each another and the numerical solution is identical to one for FM zigzag chains. Hence, the two bands have the same OAM. When $J_1 = -J_2$, the lower band exhibits a larger amplitude of the OAM than the upper band, as seen in the central panel of Fig. 2(b). When $J_2 = 0.01$ and $J_1 = -1$, the FM interaction within each zigzag chain is very weak while the AF interaction between chains is strong. Then the OAM is only significant around discrete points \mathbf{k}^* along the line $k_x = k_y$. As expected, the OAM vanishes as $J_2/|J_1| \rightarrow 0$.

(iii) *FM honeycomb*.—We now consider the honeycomb lattice shown in Fig. 3(a) with FM exchange coupling $J > 0$. Provided that the easy-axis anisotropy $-K \sum_i S_{iz}^2$ is sufficiently strong, we may also add a DM interaction D between next-neighbor sites without tilting the up spins. We then find

$$\underline{L}(\mathbf{k}) = \frac{3JS}{2} \begin{pmatrix} 1 - G_{\mathbf{k}} & -\Gamma_{\mathbf{k}}^* & 0 & 0 \\ -\Gamma_{\mathbf{k}} & 1 + G_{\mathbf{k}} & 0 & 0 \\ 0 & 0 & 1 + G_{\mathbf{k}} & -\Gamma_{\mathbf{k}}^* \\ 0 & 0 & -\Gamma_{\mathbf{k}} & 1 - G_{\mathbf{k}} \end{pmatrix}, \quad (12)$$

where $G_{\mathbf{k}} = d\Theta_{\mathbf{k}}$ with $d = -2D/3J$, $\Theta_{\mathbf{k}} = 4\cos(3k_x a/2) \times \sin(\sqrt{3}k_y a/2) - 2\sin(\sqrt{3}k_y a)$, and

$$\Gamma_{\mathbf{k}} = \frac{1}{3} \{ e^{ik_x a} + e^{-i(k_x + \sqrt{3}k_y)a/2} + e^{-i(k_x - \sqrt{3}k_y)a/2} \}. \quad (13)$$

Because the anisotropy $\kappa = 2K/3|J|$ merely shifts the magnon energies $\hbar\omega_{1,2}(\mathbf{k}) = 3JS(1 + \kappa \pm g_{\mathbf{k}})$ with $g_{\mathbf{k}} = \sqrt{|\Gamma_{\mathbf{k}}|^2 + G_{\mathbf{k}}^2}$ but does not affect the OAM, we neglect its contribution to $\underline{L}(\mathbf{k})$. After the usual manipulations, we find $X^{-1}(\mathbf{k})_{11} = -1/2c_1g_{\mathbf{k}}$, $X^{-1}(\mathbf{k})_{12} = 1/2c_2g_{\mathbf{k}}$, $X^{-1}(\mathbf{k})_{21} = (G_{\mathbf{k}} + g_{\mathbf{k}})/2c_1\Gamma_{\mathbf{k}}^*g_{\mathbf{k}}$, and $X^{-1}(\mathbf{k})_{22} = -(G_{\mathbf{k}} - g_{\mathbf{k}})/2c_2\Gamma_{\mathbf{k}}^*g_{\mathbf{k}}$, where $1/|c_1|^2 = 2g_{\mathbf{k}}(g_{\mathbf{k}} - G_{\mathbf{k}})$

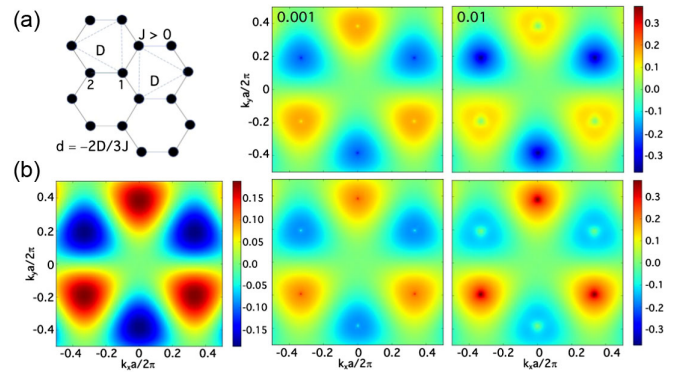


FIG. 3. FM honeycomb. (a) A honeycomb lattice with FM exchange $J > 0$ between neighboring up spins and DM interaction D between next-nearest neighbors. (b) The OAM for the upper (top) and lower (bottom) bands versus \mathbf{k} for different values of $d = -2D/3J$.

and $1/|c_2|^2 = 2g_{\mathbf{k}}(g_{\mathbf{k}} + G_{\mathbf{k}})$. The 31, 32, 41, and 42 matrix elements of $\underline{X}^{-1}(\mathbf{k})$ vanish.

For $d = 0$, the upper and lower band frequencies $\omega_1(\mathbf{k})$ and $\omega_2(\mathbf{k})$ cross at $\mathbf{k}^* = (1/3, \sqrt{3}/9)(2\pi/a)$ and equivalent points at the corners of the BZ. With

$$\mathcal{L}_{zn}(\mathbf{k}) = \frac{\hbar}{4} \frac{\Gamma_{\mathbf{k}}}{|\Gamma_{\mathbf{k}}|} \hat{l}_{z\mathbf{k}} \frac{\Gamma_{\mathbf{k}}^*}{|\Gamma_{\mathbf{k}}|}, \quad (14)$$

the OAM is the same for both bands. Notice that this expression is the same as Eq. (9) for $\mathcal{L}_{zn}(\mathbf{k})$ of the FM zigzag lattice with $\Psi_{\mathbf{k}}$ replaced by $\Gamma_{\mathbf{k}}$. As seen in Fig. 3(b), $\mathcal{L}_{zn}(\mathbf{k})/\hbar$ has modest values of $\pm 3/16 = \pm 0.1875$ at \mathbf{k}^* [21,22].

Since DM interactions change sign upon spatial inversion, $\mathcal{L}_{zn}(\mathbf{k})/\hbar$ contains both even and odd terms with respect to \mathbf{k} due to the $G_{\mathbf{k}} = -G_{-\mathbf{k}} \sim d$ functions in $\underline{X}^{-1}(\mathbf{k})$. For $d > 0$, the averages of $\mathcal{L}_{z1}(\mathbf{k})/\hbar$ and $\mathcal{L}_{z2}(\mathbf{k})/\hbar$ over the BZ are negative and positive, respectively. With increasing d , a gap opens between the two magnon bands and $|\mathcal{L}_{zn}(\mathbf{k})|$ grows at the avoided-crossings points \mathbf{k}^* . For $d = 0.01$, the largest values of the OAM at \mathbf{k}^* are about $\pm 0.38\hbar$. The Berry curvature [15] of the FM honeycomb lattice is discussed in the Supplemental Material [19].

(iv) *AF honeycomb*.—The final case study is the honeycomb lattice sketched in Fig. 4(a) with AF exchange $J < 0$ between alternating up and down spins. Since it shifts the magnon energies but does not affect the OAM, the DM interaction is neglected in the following discussion. We obtain

$$\underline{L}(\mathbf{k}) = -\frac{3JS}{2} \begin{pmatrix} 1 + \kappa & 0 & 0 & -\Gamma_{\mathbf{k}}^* \\ 0 & 1 + \kappa & -\Gamma_{\mathbf{k}} & 0 \\ 0 & -\Gamma_{\mathbf{k}}^* & 1 + \kappa & 0 \\ -\Gamma_{\mathbf{k}} & 0 & 0 & 1 + \kappa \end{pmatrix}. \quad (15)$$

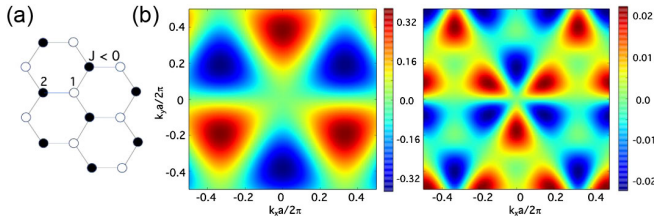


FIG. 4. AF honeycomb. (a) A honeycomb lattice with AF exchange $J < 0$ between up (closed circles, site 2) and down (open circles, site 1) spins. (b) The OAM of the major (left) and minor (right) bands versus \mathbf{k} for anisotropy $\kappa = 0$.

The usual procedure yields $X^{-1}(\mathbf{k})_{11} = -1/2c_1f_{\mathbf{k}}$, $X^{-1}(\mathbf{k})_{32} = 1/2c_2f_{\mathbf{k}}$, $X^{-1}(\mathbf{k})_{22} = (f_{\mathbf{k}} + 1 + \kappa)/2c_2\Gamma_{\mathbf{k}}^*f_{\mathbf{k}}$, and $X^{-1}(\mathbf{k})_{41} = (f_{\mathbf{k}} - 1 - \kappa)/2c_1\Gamma_{\mathbf{k}}^*f_{\mathbf{k}}$, where $1/|c_1|^2 = 2f_{\mathbf{k}}(1 + \kappa + f_{\mathbf{k}})$ and $1/|c_2|^2 = 2f_{\mathbf{k}}(1 + \kappa - f_{\mathbf{k}})$ with $f_{\mathbf{k}} = \sqrt{(1 + \kappa)^2 - |\Gamma_{\mathbf{k}}|^2}$. Other matrix elements of $X^{-1}(\mathbf{k})_{mn}$ for modes $n = 1$ and 2 vanish.

Surprisingly, the doubly degenerate magnon bands with energies $\hbar\omega_{1,2}(\mathbf{k}) = 3|J|S\sqrt{(1 + \kappa)^2 - |\Gamma_{\mathbf{k}}|^2}$ exhibit distinct OAMs with

$$\mathcal{L}_{z1}(\mathbf{k}) = \frac{\hbar}{4} \frac{1 + \kappa + f_{\mathbf{k}}}{f_{\mathbf{k}}} \frac{\Gamma_{\mathbf{k}}}{|\Gamma_{\mathbf{k}}|} \hat{\gamma}_{z\mathbf{k}} \frac{\Gamma_{\mathbf{k}}^*}{|\Gamma_{\mathbf{k}}|}, \quad (16)$$

$$\mathcal{L}_{z2}(\mathbf{k}) = -\frac{\hbar}{4} \frac{1 + \kappa - f_{\mathbf{k}}}{f_{\mathbf{k}}} \frac{\Gamma_{\mathbf{k}}}{|\Gamma_{\mathbf{k}}|} \hat{\gamma}_{z\mathbf{k}} \frac{\Gamma_{\mathbf{k}}^*}{|\Gamma_{\mathbf{k}}|}, \quad (17)$$

and ratio $\mathcal{L}_{z1}(\mathbf{k})/\mathcal{L}_{z2}(\mathbf{k}) = -(1 + \kappa + f_{\mathbf{k}})/(1 + \kappa - f_{\mathbf{k}}) < 0$. As seen in Fig. 4(b) for $\kappa = 0$, the major and minor bands have different patterns for $\mathcal{L}_{zn}(\mathbf{k})$ but are both threefold symmetric. The maxima in $|\mathcal{L}_{z1}(\mathbf{k})|/\hbar$ of $3/8$ [22] appear at points \mathbf{k}^* where $\Gamma_{\mathbf{k}}$ vanishes and $\hbar\omega_n(\mathbf{k})$ reaches a maximum of $3|J|S$. Those points coincide with the avoided-crossing points \mathbf{k}^* of the nondegenerate bands for the FM honeycomb lattice.

The average OAM $\mathcal{L}_{av}(\mathbf{k}) = [\mathcal{L}_{z1}(\mathbf{k}) + \mathcal{L}_{z2}(\mathbf{k})]/2$ of the major and minor bands of the AF honeycomb lattice equals the OAM of the $d = 0$ FM honeycomb lattice given by Eq. (14) and plotted in Fig. 3. We emphasize that the major and minor bands of the AF honeycomb lattice are identical in every other respect. For example, their spin-spin correlation functions $S_{\alpha\beta}(\mathbf{k}, \omega)$ are equal [19].

The topological nature of quasiparticles in solids is often characterized by their Berry phase [15]. In momentum space, the Berry curvature is given by

$$\Omega_n(\mathbf{k}) = \frac{i}{2\pi} \{ \nabla_{\mathbf{k}} \times \langle u_n(\mathbf{k}) | \nabla_{\mathbf{k}} u_n(\mathbf{k}) \rangle \} \cdot \mathbf{z}, \quad (18)$$

where $|u_n(\mathbf{k})\rangle$ is the single-particle wave function of band n and $\langle u_n(\mathbf{k}) | \nabla_{\mathbf{k}} u_n(\mathbf{k}) \rangle$ is called the Berry connection. Integrating $\Omega_n(\mathbf{k})$ over the BZ then gives the Chern number

\mathcal{C}_n . The relation between the Berry curvature and the OAM is clarified by rewriting Eq. (5) as

$$\mathcal{L}_{zn}(\mathbf{k}) = -\frac{i\hbar}{2} \{ \mathbf{k} \times \langle u_n(\mathbf{k}) | \nabla_{\mathbf{k}} u_n(\mathbf{k}) \rangle \} \cdot \mathbf{z}. \quad (19)$$

Thus, while the Berry curvature is the curl of the Berry connection, the OAM is the cross product of the momentum \mathbf{k} and the Berry connection.

At low energies and momenta, Eq. (19) reduces to the expression of Matsumoto and Murakami [12,13] for FM magnons, which was parameterized in terms of an effective mass m^* . Since we are interested in the OAM of both FM and AF magnons throughout the BZ, we prefer using the more general expression given above. Because it is produced by SO coupling, the OAM discussed in Ref. [5] is not related to the one described by Eq. (19).

Whenever magnons exhibit OAM, the lattice contains two inequivalent sites either due to exchange [cases (i) and (ii)] or structure [cases (iii) and (iv)]. In such a non-Bravais lattice, the violation of inversion symmetry about each site creates preferred channels for the magnons and an asymmetry in \mathbf{k} space that produces the OAM. In that sense, the present Letter follows in the spirit of earlier work on magnon confinement in spherical [6–8] and cylindrical [9–11] geometries. We surmise that it may be easier to generate and control the OAM of magnons by designing devices with tailored exchange interactions than with customized SO couplings and spin textures.

In all four case studies, the largest OAM appears at the crossing points or extremum \mathbf{k}^* of the magnon bands. For the FM zigzag lattice, a slight increase of $r = J_2/J_1$ from 1 has a huge effect on the OAM because it creates two inequivalent magnetic sites while opening a gap between the magnon bands at \mathbf{k}^* . Increasing $r > 1$ further reduces the OAM while widening the gap between the magnon bands. Since the FM honeycomb lattice with $D = 0$ already contains two inequivalent sites, its magnons exhibit non-zero OAM at wave vectors \mathbf{k}^* and elsewhere throughout the BZ. By breaking the odd symmetry of $\mathcal{L}_{zn}(\mathbf{k})$, a nonzero D allows the upper and lower magnon bands to carry a net OAM when averaged over the BZ. Consequently, larger values of the OAM appear at \mathbf{k}^* . Because it breaks the degeneracy of otherwise identical bands, the OAM of an AF honeycomb lattice is particularly intriguing.

This Letter opens the gateway for the future experimental study of the OAM of magnons in collinear spin systems. While bulk zigzag systems with $J_1 \approx J_2 > 0$ [case (i)] are difficult to experimentally identify due to their similar exchange constants, many experimental systems can be described as zigzags coupled by AF exchange $J_1 < 0$ [case (ii)]. AF-coupled zigzag chains decorate the quasi-two-dimensional honeycomb lattice compound $\text{Na}_2\text{Co}_2\text{TeO}_6$ [23], the transition-metal thiophosphates XPS_3 ($X = \text{Fe}$ or Ni) [24–26], and iridium-based compounds like Na_2IrO_3 [27]. Both the honeycomb sublattice of $\text{Li}_3\text{Ni}_2\text{SbO}_6$ [28]

and the square AF sublattice of $\text{Ba}_2\text{Mn}(\text{PO}_4)_2$ [29] also contain zigzag chains. While many Ruddlesden-Popper manganites have zigzag chains with AF correlations [30], the metallic manganite $\text{La}_{0.67}\text{Ca}_{0.33}\text{MnO}_3$ has zigzag chains running within square AF ab planes [31]. Because of their photoluminescent properties, many of these materials are candidates for optospintronics, which provides avenues to probe or perturb the OAM of magnons.

The magnetic phase diagrams of honeycomb systems with chemical formula ABX_3 were reviewed by Sivadas *et al.* [32]. Examples of FM honeycomb lattices [case (iii)] are CrSiTe_3 and CrGeTe_3 [33–35]. Another well-known Cr-based FM honeycomb system is CrI_3 [36], which has topological magnon excitations that were studied by Chen *et al.* [37]. CrCl_3 has recently joined this family [38]. AF honeycomb lattices [case (iv)] are found in MnPS_3 and MnPSe_3 [39].

Most measurements do not probe the OAM of magnons because $\mathcal{L}_{zn}(\mathbf{k})$ averages to zero when \mathbf{k} is summed over the BZ and n is summed over all magnon bands. One possible experiment to probe the OAM of magnons is sketched in Fig. 1(d), where a temperature gradient [40] separates magnons with momenta $\pm\mathbf{k}$ and OAM $\pm\mathcal{L}$ for a FM zigzag lattice where $\mathcal{L}_{zn}(\mathbf{k}) = -\mathcal{L}_{zn}(-\mathbf{k})$. To prevent magnons from establishing local thermal equilibrium, the region of temperature $T + \Delta T$ must have dimensions comparable to the spin diffusion length [41].

An alternate experiment could use a FM honeycomb lattice with DM interaction D . Because $\mathcal{L}_{zn}(\mathbf{k}) \neq -\mathcal{L}_{zn}(-\mathbf{k})$, $\langle \mathcal{L}_{zn}(\mathbf{k}) \rangle \neq 0$ in both the upper and lower magnon bands. Since a thermal average will favor the lower band, magnons in the diffusive limit will travel with $\langle \mathcal{L}_z \rangle > 0$ both to the right and to the left in Fig. 1(d), thereby opposing the magnon spin $\mathcal{S}_z = -\hbar$.

Once a magnon with momentum \mathbf{k} and OAM $\mathcal{L}_{zn}(\mathbf{k})$ is created, total angular momentum $\mathcal{J}_z = \mathcal{S}_z + \mathcal{L}_z$ is conserved due to dipolar interactions [16,17] even in the absence of SO coupling. There are many physical consequences connected with the predicted OAM of magnons, such as its effect on magnon decay rates and the scattering of magnons by photons [42] and phonons [43–45] carrying OAM. While numerous issues remain to be explored, including the generalization of this Letter for noncollinear spin states, we have established that the magnons of two-dimensional collinear magnets can carry significant OAM provided that the exchange interactions meet some easily satisfied conditions. We hope that this Letter helps magnonics join fields such as optics [46–48] and “orbitronics” [49–51] where OAM now plays an important role.

The data that support the findings of this study are available from the corresponding author upon reasonable request. The DOE will provide public access to these results of federally sponsored research in accordance with the DOE Public Access Plan [52].

We acknowledge useful conversations with D. Xiao and R. deSousa. Research sponsored by the Laboratory Directors Fund of Oak Ridge National Laboratory. This Letter has been authored in part by UT-Battelle, LLC, under Contract No. DE-AC05-00OR22725 with the US Department of Energy (DOE). The US government retains and the publisher, by accepting the article for publication, acknowledges that the US government retains a nonexclusive, paid-up, irrevocable, worldwide license to publish or reproduce the published form of this manuscript, or allow others to do so, for US government purposes.

*Corresponding author.
fishmanrs@ornl.gov

- [1] A. Einstein and W. J. de Hass, Experimental proof of the existence of Ampere’s molecular currents, *Verh. Dtsch. Phys. Ges.* **17**, 152 (1915).
- [2] S. J. Barnett, Magnetization by rotation, *Phys. Rev.* **6**, 239 (1915).
- [3] Strictly speaking, the orbital angular momentum of a crystal discussed in this Letter is the “pseudo” orbital angular momentum [4] because rotational invariance is violated in a lattice.
- [4] Simon Streib, Difference between angular momentum and pseudoangular momentum, *Phys. Rev. B* **103**, L100409 (2021).
- [5] Robin R. Neumann, Alexander Mook, Jürgen Henk, and Ingrid Mertig, Orbital Magnetic Moment of Magnons, *Phys. Rev. Lett.* **125**, 117209 (2020).
- [6] J. A. Haigh, A. Nunnenkamp, A. J. Ramsay, and A. J. Ferguson, Triple-Resonant Brillouin Light Scattering in Magneto-Optical Cavities, *Phys. Rev. Lett.* **117**, 133602 (2016).
- [7] Sanchar Sharma, Yaroslav M. Blanter, and Gerrit E. W. Bauer, Light scattering by magnons in whispering gallery mode cavities, *Phys. Rev. B* **96**, 094412 (2017).
- [8] A. Osada, A. Gloppe, Y. Nakamura, and K. Usami, Orbital angular momentum conservation in brillouin light scattering within a ferromagnetic sphere, *New J. Phys.* **20**, 103018 (2018).
- [9] Yuanyuan Jiang, H. Y. Yuan, Z.-X. Li, Zhenyu Wang, H. W. Zhang, Yunshan Cao, and Peng Yan, Twisted Magnon as a Magnetic Tweezer, *Phys. Rev. Lett.* **124**, 217204 (2020).
- [10] Seungho Lee and Se Kwon Kim, Generation of magnon orbital angular momentum by a skyrmion-textured domain wall in a ferromagnetic nanotube, *Front. Phys.* **10**, 858614 (2022).
- [11] E. O. Kamenetskii, Magnetic dipolar modes in magnon-polariton condensates, *J. Mod. Opt.* **68**, 1147 (2021).
- [12] Ryo Matsumoto and Shuichi Murakami, Theoretical Prediction of a Rotating Magnon Wave Packet in Ferromagnets, *Phys. Rev. Lett.* **106**, 197202 (2011).
- [13] Ryo Matsumoto and Shuichi Murakami, Rotational motion of magnons and the thermal hall effect, *Phys. Rev. B* **84**, 184406 (2011).

- [14] Jun Li, Trinanjan Datta, and Dao-Xin Yao, Einstein-de Haas effect of topological magnons, *Phys. Rev. Res.* **3**, 023248 (2021).
- [15] Di Xiao, Ming-Che Chang, and Qian Niu, Berry phase effects on electronic properties, *Rev. Mod. Phys.* **82**, 1959 (2010).
- [16] V. M. Tsukernik, Some features of the gyromagnetic effect in ferroelectrics at low temperatures, *Sov. J. Exp. Theor. Phys.* **50**, 1631 (1966).
- [17] V. S. Garmatyuk and V. M. Tsukernik, The gyromagnetic effect in an antiferromagnet at low temperatures, *Sov. J. Exp. Theor. Phys.* **26**, 1035 (1968).
- [18] L. D. Landau and E. M. Lifshitz, *The Classical Theory of Fields*, Fourth revised english ed. (Butterworth-Heinemann, Oxford, 1973).
- [19] See Supplemental Material at <http://link.aps.org/supplemental/10.1103/PhysRevLett.129.167202> for a derivation of semiclassical expression for OAM, symmetry relations for the FM zig-zag lattice, a discussion of the Berry curvature, and a derivation of the periodic functions \bar{k}_x and \bar{k}_y .
- [20] Randy S. Fishman, Jaime Fernandez-Baca, and Toomas Rõõm, *Spin-Wave Theory and Its Applications to Neutron Scattering and THz Spectroscopy* (Morgan and Claypool Publishers, San Rafael, 2018).
- [21] To assure that $\mathcal{L}_{zn}(\mathbf{k})$ is periodic in the BZ, we must make sure that the wave vectors used in its definition are periodic. Recalling that k_x and k_y originate from the continuous derivatives $-i\partial/\partial x$ and $-i\partial/\partial y$, respectively, we replace the continuous derivatives by discrete finite differences as detailed in Supplementary Material [19].
- [22] R. S. Fishman, L. Lindsay, and S. Okamoto, Exact results for orbital angular momentum of magnons at the high symmetry points of honeycomb magnets, [arXiv:2207.09883](https://arxiv.org/abs/2207.09883).
- [23] A. K. Bera, S. M. Yusuf, Amit Kumar, and C. Ritter, Zigzag antiferromagnetic ground state with anisotropic correlation lengths in the quasi-two-dimensional honeycomb lattice compound $\text{Na}_2\text{Co}_2\text{TeO}_6$, *Phys. Rev. B* **95**, 094424 (2017).
- [24] A. R. Wildes, V. Simonet, E. Ressouche, G. J. McIntyre, M. Avdeev, E. Suard, S. A. J. Kimber, D. Lançon, G. Pepe, B. Moubaraki, and T. J. Hicks, Magnetic structure of the quasi-two-dimensional antiferromagnet NiPS_3 , *Phys. Rev. B* **92**, 224408 (2015).
- [25] D. Lançon, H. C. Walker, E. Ressouche, B. Ouladdiaf, K. C. Rule, G. J. McIntyre, T. J. Hicks, H. M. Rønnow, and A. R. Wildes, Magnetic structure and magnon dynamics of the quasi-two-dimensional antiferromagnet FePS_3 , *Phys. Rev. B* **94**, 214407 (2016).
- [26] Qi Zhang, Kyle Hwangbo, Chong Wang, Qianni Jiang, Jiun-Haw Chu, Haidan Wen, Di Xiao, and Xiaodong Xu, Observation of giant optical linear dichroism in a zigzag antiferromagnet FePS_3 , *Nano Lett.* **21**, 6938 (2021).
- [27] Feng Ye, Songxue Chi, Huibo Cao, Bryan C. Chakoumakos, Jaime A. Fernandez-Baca, Radu Custelean, T. F. Qi, O. B. Korneta, and G. Cao, Direct evidence of a zigzag spin-chain structure in the honeycomb lattice: A neutron and x-ray diffraction investigation of single-crystal Na_2IrO_3 , *Phys. Rev. B* **85**, 180403(R) (2012).
- [28] A. I. Kurbakov, A. N. Korshunov, S. Yu. Podchertsev, A. L. Malyshev, M. A. Evstigneeva, F. Damay, J. Park, C. Koo, R. Klingeler, E. A. Zvereva, and V. B. Nalbandyan, Zigzag spin structure in layered honeycomb $\text{Li}_3\text{Ni}_2\text{SbO}_6$: A combined diffraction and antiferromagnetic resonance study, *Phys. Rev. B* **96**, 024417 (2017).
- [29] Arvind Yogi, A. K. Bera, Ashwin Mohan, Ruta Kulkarni, S. M. Yusuf, A. Hoser, A. A. Tsirlin, M. Isobe, and A. Thamizhavel, Zigzag spin chains in the spin-5/2 antiferromagnet $\text{Ba}_2\text{Mn}(\text{PO}_4)_2$, *Inorg. Chem. Front.* **6**, 2736 (2019).
- [30] Myron B. Salamon and Marcelo Jaime, The physics of manganites: Structure and transport, *Rev. Mod. Phys.* **73**, 583 (2001).
- [31] Nikolaos Panopoulos, M. Pissas, H. J. Kim, J.-G. Kim, Seung J. Yoo, J. Hassan, Y. AlWahedi, S. Alhassan, M. Fardis, N. Boukos, and G. Papavassiliou, Polaron freezing and the quantum liquid-crystal phase in the ferromagnetic metallic $\text{La}_{0.67}\text{Ca}_{0.33}\text{MnO}_3$, *npj Quantum Mater.* **3**, 20 (2018).
- [32] Nikhil Sivadas, Matthew W. Daniels, Robert H. Swendsen, Satoshi Okamoto, and Di Xiao, Magnetic ground state of semiconducting transition-metal trichalcogenide monolayers, *Phys. Rev. B* **91**, 235425 (2015).
- [33] V. Carteaux, F. Moussa, and M. Spiesser, 2d Ising-like ferromagnetic behaviour for the lamellar CrSi_2Te_6 compound: A neutron scattering investigation, *Europhys. Lett.* **29**, 251 (1995).
- [34] V. Carteaux, D. Brunet, G. Ouvrard, and G. Andre, Crystallographic, magnetic and electronic structures of a new layered ferromagnetic compound $\text{Cr}_2\text{Ge}_2\text{Te}_6$, *J. Phys. Condens. Matter* **7**, 69 (1995).
- [35] L. D. Casto, A. J. Clune, M. O. Yokosuk, J. L. Musfeldt, T. J. Williams, H. L. Zhuang, M.-W. Lin, K. Xiao, R. G. Hennig, B. C. Sales, J.-Q. Yan, and D. Mandrus, Strong spin-lattice coupling in CrSiTe_3 , *APL Mater.* **3**, 041515 (2015).
- [36] Michael A. McGuire, Hemant Dixit, Valentino R. Cooper, and Brian C. Sales, Coupling of crystal structure and magnetism in the layered, ferromagnetic insulator CrI_3 , *Chem. Mater.* **27**, 612 (2015).
- [37] Lebing Chen, Jae-Ho Chung, Bin Gao, Tong Chen, Matthew B. Stone, Alexander I. Kolesnikov, Qingzhen Huang, and Pengcheng Dai, Topological Spin Excitations in Honeycomb Ferromagnet CrI_3 , *Phys. Rev. X* **8**, 041028 (2018).
- [38] X. Li, S. Do, J. Yan, M. McGuire, G. Granroth, S. Mu, T. Berlijn, V. Cooper, A. Christianson, and L. Lindsay, Phonons and phase symmetries in bulk CrCl_3 from scattering measurements and theory, [arXiv:2209.02394](https://arxiv.org/abs/2209.02394).
- [39] A. R. Wildes, B. Roessli, B. Lebech, and K. W. Godfrey, Spin waves and the critical behaviour of the magnetization in MnPS_3 , *J. Phys. Condens. Matter* **10**, 6417 (1998).
- [40] Ran Cheng, Satoshi Okamoto, and Di Xiao, Spin Nernst Effect of Magnons in Collinear Antiferromagnets, *Phys. Rev. Lett.* **117**, 217202 (2016).
- [41] Hantao Zhang and Ran Cheng, Spin Nernst Effect of Antiferromagnetic Magnons in the Presence of Spin Diffusion, *Phys. Rev. Appl.* **16**, 034035 (2021).

- [42] L. Marrucci, C. Manzo, and D. Paparo, Optical Spin-to-Orbital Angular Momentum Conversion in Inhomogeneous Anisotropic Media, *Phys. Rev. Lett.* **96**, 163905 (2006).
- [43] Lifa Zhang and Qian Niu, Angular Momentum of Phonons and the Einstein–de Haas Effect, *Phys. Rev. Lett.* **112**, 085503 (2014).
- [44] Lifa Zhang and Qian Niu, Chiral Phonons at High-Symmetry Points in Monolayer Hexagonal Lattices, *Phys. Rev. Lett.* **115**, 115502 (2015).
- [45] Masato Hamada, Emi Minamitani, Motoaki Hirayama, and Shuichi Murakami, Phonon Angular Momentum Induced by the Temperature Gradient, *Phys. Rev. Lett.* **121**, 175301 (2018).
- [46] Yijie Shen, Xuejiao Wang, Zhenwei Xie, Changjun Min, Xing Fu, Qiang Liu, Mali Gong, and Xiaocong Yuan, Optical vortices 30 years on: OAM manipulation from topological charge to multiple singularities, *Light* **8**, 90 (2019).
- [47] Yiqi Fang, Shengyue Lu, and Yunquan Liu, Controlling Photon Transverse Orbital Angular Momentum in High Harmonic Generation, *Phys. Rev. Lett.* **127**, 273901 (2021).
- [48] Guillermo F. Quinteiro Rosen, Pablo I. Tamborenea, and Tilmann Kuhn, Interplay between optical vortices and condensed matter, *Rev. Mod. Phys.* **94**, 035003 (2022).
- [49] Dongwook Go, Daegeun Jo, Hyun-Woo Lee, Mathias Klui, and Yuriy Mokrousov, Orbitronics: Orbital currents in solids, *Europhys. Lett.* **135**, 37001 (2021).
- [50] Seungyun Han, Hyun-Woo Lee, and Kyoung-Whan Kim, Orbital Dynamics in Centrosymmetric Systems, *Phys. Rev. Lett.* **128**, 176601 (2022).
- [51] Oliver Dowinton and Mohammad Saeed Bahramy, Orbital angular momentum driven anomalous hall effect, *Phys. Rev. B* **105**, 235142 (2022).
- [52] <http://energy.gov/downloads/doi-public-access-plan>.